frontiers | Frontiers in Materials

TYPE Original Research
PUBLISHED 03 November 2022
DOI 10.3389/fmats.2022.1054725

Check for updates

OPEN ACCESS

EDITED BY
Reza Peymanfar,
Energy Institute of Higher Education, Iran

REVIEWED BY
Guangbin Ji,
Nanjing University of Aeronautics and Astronautics, China
Mao-Sheng Cao,
Beijing Institute of Technology, China
Bagher Aslibeiki,
University of Tabriz, Iran

*CORRESPONDENCE
Jianbo Wang,
wangjb@lzu.edu.cn

SPECIALTY SECTION
This article was submitted to Polymeric and Composite Materials, a section of the journal Frontiers in Materials

RECEIVED 27 September 2022
ACCEPTED 20 October 2022
PUBLISHED 03 November 2022

CITATION
Li X, Qiao L, Shi H, Chai G, Wang T and Wang J (2022), Temperature denpendent microwave absorption properties of $SrFe_{12}O_{19}$ in X-band. *Front. Mater.* 9:1054725. doi: 10.3389/fmats.2022.1054725

COPYRIGHT
© 2022 Li, Qiao, Shi, Chai, Wang and Wang. This is an open-access article distributed under the terms of the Creative Commons Attribution License (CC BY). The use, distribution or reproduction in other forums is permitted, provided the original author(s) and the copyright owner(s) are credited and that the original publication in this journal is cited, in accordance with accepted academic practice. No use, distribution or reproduction is permitted which does not comply with these terms.

Temperature denpendent microwave absorption properties of $SrFe_{12}O_{19}$ in X-band

Xiling Li[1,2,3], Liang Qiao[1,2], Huigang Shi[1], Guozhi Chai[1,2], Tao Wang[1,2] and Jianbo Wang[1,2]*

[1]Key Laboratory for Magnetism and Magnetic Materials of the Ministry of Education, Lanzhou University, Lanzhou, China, [2]Key Laboratory for Special Function Materials and Structural Design of the Ministry of Education, Lanzhou University, Lanzhou, China, [3]National Demonstration Center for Experimental Physics Education, Lanzhou University, Lanzhou, China

Researchers are currently focusing on the electromagnetic and microwave absorption properties of $SrFe_{12}O_{19}$ hexaferrites. The high-temperature absorption (more than 573 K) is highly demanded in various including the military, national defense, aviation, and other fields. $SrFe_{12}O_{19}$ has good thermal stability at high temperature, and it has large coercivity, which also determines that it has good stability in magnetic properties and is not easy to be affected by the environment. Thus, it is necessary to explore the magnetic characteristics of $SrFe_{12}O_{19}$ hexaferrites at high temperatures. $SrFe_{12}O_{19}$ hexaferrites were fabricated by the molten salt method and their microstructure, high-temperature electromagnetic properties, and microwave properties were investigated in detail. The complex permeability and permittivity of $SrFe_{12}O_{19}$ were measured at varying temperatures (293–673 K) in the X band. While the real parts of permittivity and permeability increased with the increasing temperature, the imaginary parts of permittivity and permeability did not change significantly with increasing temperature. The calculated absorption properties displayed that as temperature increased from 293K to 623K, the frequency of the RL peaks moved to a low-frequency direction, and the sample's minimum value of RL could be smaller than -10dB across the whole X band. The results indicate that $SrFe_{12}O_{19}$ particles have better absorption properties and can be used in high-temperature environments. These particles can be possibly used in many particular fields.

KEYWORDS

$SrFe_{12}O_{19}$, microwave absorption properties, electromagnetic properties, high temperature, X band, reflection loss

Introduction

Microwave absorption materials are widely used in computers, communication, household appliances, national defense, and military fields, especially in the GHz band. Consequently, the investigation into the microwave absorption capabilities of materials has always been a major concern. The electromagnetic parameter is directly

related to the microwave absorption capabilities of absorbent materials. Efforts have been made to improve high-frequency electromagnetic efficiency as demands for GHz-band microwave absorbers have grown significantly (Li et al., 2014; Mehdipour and Shokrollahi, 2013; Zheng et al., 2016; Li et al., 2015). Therefore, it is essential to use a stable magnetic material. As absorbing materials, ferrites and metallic magnetic materials with a magnetic loss mechanism have been extensively studied (Mehdipour and Shokrollahi, 2013; Zheng et al., 2016; Li et al., 2015). Typically, metallic magnetic materials have a low resistivity, which could lead to a significant eddy current loss in the GHz frequency range, hence limiting their technological applications. Meanwhile, ferrites are considered to be the optimal choice for industrial applications due to their high resistivity, minimal eddy current loss, high saturation magnetization, and outstanding electromagnetic characteristics (Tang et al., 2016; Zhang et al., 2016; Ye et al., 2015).

Due to the Snoek's limit, the cut-off frequency for typical soft spinel ferrite, such as $NiZnFe_2O_4$ or $MnFe_2O_4$, is as low as a few MHz despite the material's considerable permeability at low frequencies (Ghasemi and Mousavinia, 2014). However, to obtain a ferrite with a high cut-off frequency, the effective anisotropy field must be increased. As M-type $SrFe_{12}O_{19}$ is a typical hexagonal ferrite, with a high magnetocrystalline anisotropy field that is primarily used as a permanent magnet material due to its high coercive force, relatively high saturation magnetization, and high Curie temperature, as well as its high dielectric loss, good chemical stability, and corrosion resistance, it has attracted the attention of researchers, especially, about their electromagnetic and microwave absorption properties [Nie et al., 2010; Wang et al., 2001; Ghasemi et al., 2006; Zi et al., 2009; Fathi et al., 2020]. Due to the thermal impacts of the devices or particular working requirements for high-temperature, microwave devices typically run at temperatures greater than room temperature. Thus, it is necessary to explore microwave absorption performance of absorbing materials at high temperatures (Cao et al., 2010; Luo et al., 2017; Shi et al., 2008; Yuan et al., 2017). Many research groups use pure dielectric materials with outstanding thermal stability as absorbing materials, such as graphite, carbon nanosheets, SiC fiber, $BiFeO_3$ and so on, to study their microwave absorption performance at high temperature (Shi et al., 2008; Song et al., 2009; Li et al., 2015; Li et al., 2016; Lu et al., 2016; Li et al., 2018; Li et al., 2019; Yuan et al., 2017; Guan et al., 2022; Li et al., 2022; Mu et al., 2022). It is reported that all the RL can exceed -10 dB in the whole X band at elevated temperature (573–873 K). $SrFe_{12}O_{19}$ has good thermal stability at high temperature, and it has large coercivity, which also determines that it has good stability in magnetic properties and is not easy to be affected by the environment. Therefore, it is necessary to study the high-temperature absorption of $SrFe_{12}O_{19}$. However, currently, there is no research on its high-temperature electromagnetic and wave absorption characteristics. This is due to the difficulty of conducting research at ultra-high temperatures, the necessity of highly specialized equipment, and that this kind of test is not mature. Since it is still in the research phase, no commercially available direct-use equipment is available. Therefore, we have built a set of equipment that can test high-temperature electromagnetic parameters to study the related properties of magnetic materials.

In this work, M-type $SrFe_{12}O_{19}$ was prepared by the molten salt method. M-type $SrFe_{12}O_{19}$ powder and polymer were thoroughly mixed, pressed into blocks, subjected to high-temperature sintering to volatilize the polymer, and then ferrite blocks were produced. The electromagnetic properties and $SrFe_{12}O_{19}$ microwave absorption were then examined in the entire X band at temperatures ranging from 293 K to 673 K.

Experiment

$SrFe_{12}O_{19}$ was obtained by the molten salt method, and the raw materials used in the experiment were strontium carbonate ($SrCO_3$, 99%), and ferric oxide (Fe_2O_3, 99%). The mass fraction of Fe_2O_3 and $SrCO_3$ is 82.64% and 17.36% respectively. The molecular formula of M-type ferrite is $MFe_{2n}O_{19}$, and the structure of ferrite can be determined that $n = 6$ in theory, but the value of n is less than six in the actual configuration process. This is because some iron-containing substances on the ball milling tank will be ground into the ingredients in the process of ball milling, resulting in an increase in the content of iron in the ingredients. The weighed raw materials were added to the ball mill tank along with the appropriate amount of alcohol, and the mixture was allowed to mix for around 30 min. A suitable amount of alcohol was then added after mixing. Total alcohol mass to raw material mass was around 1.5:1. The ball grinding tank was placed in a planetary ball mill with a revolving speed of 200 r/min. After 2 h of ball grinding, 10% cosolvent was added, and the abrasive was placed in an oven to dry at 80°C. After drying, a small amount of dry powder was placed in a muffle furnace and prefired at different prefiring temperatures at a heating rate of 5°C/min. The prefiring temperatures were respectively 1,140°C, 1,160°C, 1,180°C, and 1,200°C for 2 h. After the holding was completed, turn off the power and allow the sample to drop to room temperature with the furnace. Finally, the cosolvent in the sample was washed with distilled water after grinding, and the sample was air dried to obtain strontium ferrite powder. Single phase M-type strontium ferrite can be prepared at all pre-firing temperature points. With the same formula, that is, the same iron content, the higher the

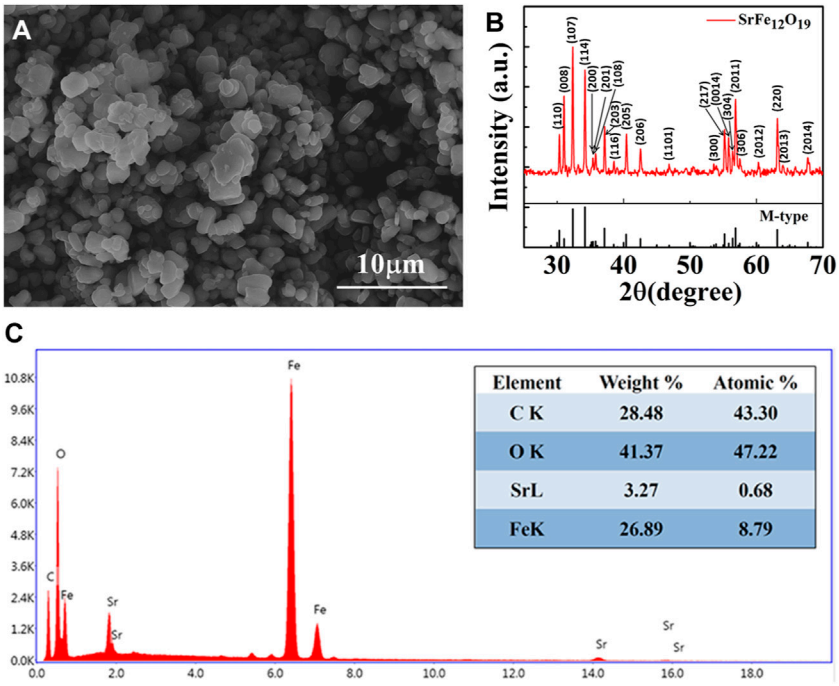

FIGURE 1
(A) SEM of $SrFe_{12}O_{19}$. **(B)** X-ray diffraction pattern of $SrFe_{12}O_{19}$. **(C)** EDS spectra and elemental mappings of the sample.

temperature, the sharper the diffraction peak, and the stronger the intensity, indicating that the higher the temperature, the better the crystallization of the sample, and the smaller the diameter thickness ratio. However, the diffraction Angle corresponding to the diffraction peak does not change, indicating that the increase of the prefiring temperature has no obvious effect on the lattice constant. Therefore, in this paper, the sample with a prefiring temperature of 1,200°C was selected as the research object. The crystallographic and microstructure properties of $SrFe_{12}O_{19}$ were analyzed by the X-ray diffractometer (XRD, X'Pert Pro PANalytical with Cu Kα radiation) and scanning electron microscope (SEM, MIRA3 TESCAN), respectively. The static magnetic characteristics of $SrFe_{12}O_{19}$ were measured at elevated temperatures using a vibrating sample magnetometer (VSM, Micro Sense VSM-EV9). The electromagnetic properties (complex permittivity and permeability) of the composite at high temperature were determined using the waveguide technique and a vector network analyzer (VNA, Agilent E8363B) in the 8.2–12.4 GHz frequency range. The samples for this assessment were made as follows: Hexaferrites were mixed with polyvinyl alcohol (the hexaferrites to paraffin weight ratio was 5:1), and then pressed into a rectangle flake with length (22.80 mm), width (10.16 mm), and thickness (2 mm) at 6 Mpa. Finally, it was heated to 1473 K in an argon atmosphere and kept there for 2 h.

Results and Discussion

Crystal structure, phase, and component

SEM images of $SrFe_{12}O_{19}$ samples are shown in Figure 1A, demonstrating that the sample has a more regular shape and structure, as well as good particle uniformity. The police force's morphology had a regular hexagonal structure, and the particle diameter thickness ratio is lower. The morphology of $SrFe_{12}O_{19}$ particles and the standard M phase (PDF 33–1,340) is shown in Figure 1B, demonstrating that $SrFe_{12}O_{19}$ is the primary phase presented by the XRD pattern. The results showed that the diffraction peak is highly sharp and intense, indicating that the sample crystallinity is very good, and the $SrFe_{12}O_{19}$ generated by this approach is a M-type hexagonal ferrite phase. Figure 1C displays the atomic percentages of various constituent elements resulting from quantitative EDS analysis for the $SrFe_{12}O_{19}$ particles, revealing that the molecular formula and the atomic ratios of Sr and Fe are in good agreement.

The static magnetic characteristics at high temperature

The hysteresis loop of $SrFe_{12}O_{19}$ measured at different temperatures is depicted in Figure 2A, which reveals that the

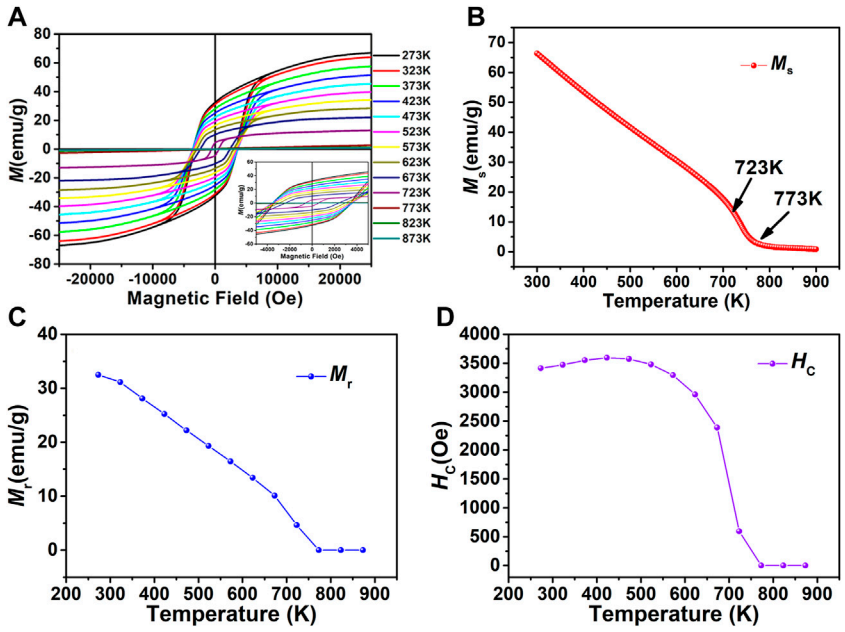

FIGURE 2
(A) Magnetic hysteresis loops of the sample. **(B)** Diagram of saturation magnetization with temperature of the sample. **(C)** Diagram of remanent magnetization with temperature of the sample. **(D)** Diagram of coercivity field with temperature of the sample.

saturation magnetization decreased gradually with temperature increase, then rapidly with temperature increase below the Curie temperature, until they became zero. At elevated temperatures, saturation magnetization and remanent magnetization gradually declined as temperature increased; when the temperature reached 723K, it dropped rapidly; and when the temperature continued to rise to 773K (Figures 2B,C), the original ferrimagnetic phase transformed into the paramagnetic phase. However, the coercivity firstly increased and then decreased gradually declined as temperature increased; when the temperature continued to rise to 773K, it decreased to zero (Figure 2D). According to the theory of the spontaneous magnetization process, when the temperature rises, the atomic distance increases, reducing the exchange effect. In addition, as a result of the law of thermal motion's continual destruction of the atomic magnetic moment's orientation, the saturation intensity of spontaneous magnetization decreases until the temperature exceeds the Curie point. This leads to the destruction of the atomic magnetic moment's regular orientation, the absence of the spontaneous magnetic moment, and the transition of the material from the ferrimagnetic phase to the paramagnetic phase.

Electromagnetic parameters at elevated temperature

High-temperature electromagnetic parameters are mostly examined using specifically designed testing equipment (Nayak et al., 2013). The test system consists primarily of a vector network analyzer, a high-temperature variable and temperature control system, a water cooling circulation system, an X-band high-temperature calibration kit, a high-temperature insulation waveguide, and a constant temperature waveguide with a water tank, and other accessories. The vector network analyzer is connected to the high-temperature insulation waveguide by a rigid cable, and the waveguide is put in a temperature box heated by radiation. Simultaneously, the cooling water circulation system is connected to the connection between the waveguide end and the cable, and the temperature at the cable connection point is rapidly lowered. Figure 3 depicts a waveguide technique high-temperature test device. The center 100 mm of the furnace is a constant-temperature zone that may accommodate the needs of high-temperature testing. Both ends are linked to the cooling water pipe, as illustrated in Figure 3.

The Thru-Reflect-Line (TRL) calibration method is selected (Stumper, and Schrader, 2014), and the supporting high-temperature calibration components and test fixtures are depicted in Figure 3. The entire device is then linked and ready for use. First, the test device was calibrated at room temperature. Secondly, in this calibrated state, the temperature was increased, and then the S_{cavity} parameter of the cavity at different temperature points was tested. In the third step, when the temperature dropped to room temperature, the sample was

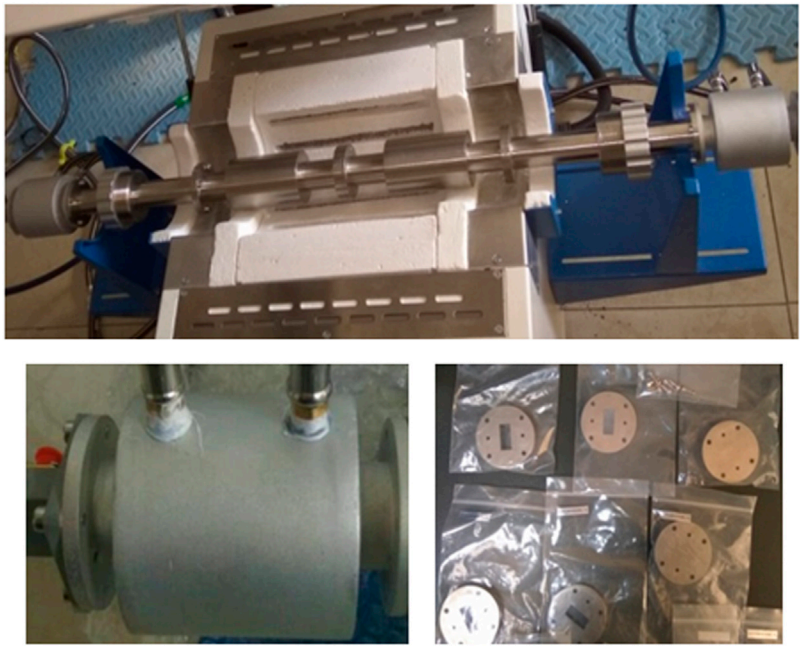

FIGURE 3
Waveguide method high-temperature test device, local magnification of water cooling part, high-temperature calibration kit, and test fixture.

put into the test fixture, and the S_{total} parameter at different temperature points was tested by increasing the temperature, so $S_{sample} = S_{total} - S_{cavity}$, then the real S_{sample} parameter of the sample at different temperature points was obtained. In the last step, the characteristic spectral lines of electromagnetic parameters varying with frequency at different temperature points were calculated according to the S_{sample} parameter.

The frequency dependency of the complex permittivity of $SrFe_{12}O_{19}$ in the X band at high temperature is illustrated in Figures 4A,B. The results indicated that the real part (ε') of permittivity increases with temperature from 9.43 at 273K to 15.37 at 673K at 8.2GHz, however, the imaginary part (ε'') does not change much with temperature. It can also be analyzed that both ε' and ε'' at varying temperatures, maintain the diagram's basic consistency. Debye's theory helps explain the dependence of permittivity on temperature (Atwater and Wheeler, 2004),

$$\varepsilon' = \varepsilon_{\infty} + \frac{\varepsilon_S - \varepsilon_{\infty}}{1 + (\omega\tau(T))^2}, \quad (1)$$

$$\varepsilon''(\omega) = \frac{\varepsilon_S - \varepsilon_{\infty}}{1 + (\omega\tau(T))^2}\omega\tau(T), \quad (2)$$

where ω represents angular frequency, τ(T) represents temperature based on relaxing time, ε_S is static permittivity, and ε_{∞} is the relative permittivity at the limit of high frequency. In accordance with the Arrhenius formula (Correia and Ramos, 2000), the τ(T) reduces as temperature rises. According to Eq. 1, a decrease in τ(T) leads to an increase in ε'. In addition, for oxide materials, because the frequency of dielectric relaxation is very high, and the test frequency is significantly lower than the resonance frequency, so ε'' tends to zero. Therefore, ε'' have no evident changes as the temperature changes.

It is known that the ε' and ε'' represent the ability of dielectric materials to store and dissipate electric energy, respectively. Additionally, the dielectric loss can be used to describe the capacity for dissipating electrical energy. The results show that its electric energy storage is excellent over the whole temperature range, below the phase transition temperature. The ε'' of all the samples are relatively small, and they do not exhibit any discernible variations in temperature over their whole range. As a result, the findings indicate that these hexaferrites have extremely little dielectric loss.

The frequency dependence of complex permeability of $SrFe_{12}O_{19}$ in the X band at high temperature is depicted in Figures 4C,D. The results show that the permeability of the real part (μ') increases with temperature from 1.16 at 273K to 2.17 at 673K at 8.2GHz, but the imaginary part (μ'') does not change much with temperature. According to the Hopkinson effect (Buzinaro et al., 2016), the magnetic

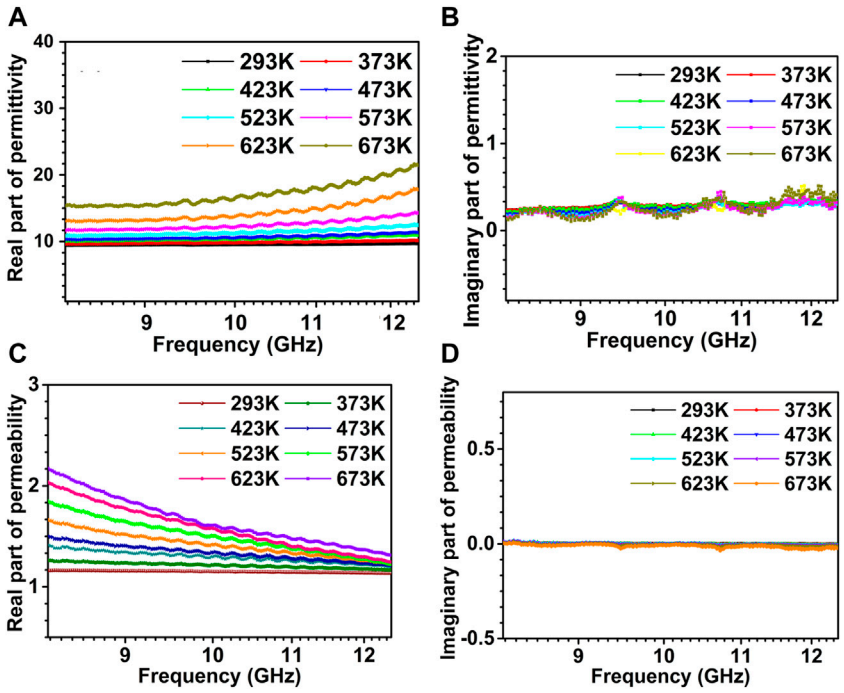

FIGURE 4
The results of the VNA samples were summarized. Frequency dependence of the real part **(A)** and imaginary part of the complex permittivity **(B)**. Frequency dependence of the real part **(C)** and imaginary part of the complex permeability **(D)**.

materials' magnetocrystalline anisotropy constant will reduce as the temperature rise, which results in a decrease in the effective field's overall magnetocrystalline anisotropy, hence μ' increases as the temperature rises. Furthermore, because the sample's magnetocrystalline anisotropic effective field is very strong, its resonance frequency is quite high; yet, the test frequency is significantly lower than the resonance frequency, so μ'' tends to zero. Therefore, μ'' are unaffected by variations in temperature.

Microwave absorption performance

The absorption property of materials is extremely important for certain application scenarios, in which absorbing materials must operate at extremely high temperatures; therefore, it is necessary to investigate whether absorbing materials retain their excellent absorption property at such temperatures. The RL represents the sample absorption characteristics for microwaves. The RL values were calculated with the complex μ and ε at given thickness d and frequency f based on the transmission line theory (Buzinaro et al., 2016). When μ and ε values are measured at different temperatures, RL values at corresponding temperatures can be calculated. The RL can be calculated as a function of the input impedance once it has been normalized, as shown in ref. [26] (Naito and Suetake, 1971):

$$RL = 20\log\left|\frac{Z_{in} - Z_0}{Z_{in} + Z_0}\right|, \tag{3}$$

Typically, the following calculation can be used to calculate the normalized input impedance, Z_{in}, of a metal-backed microwave absorption layer (Wessling, 1991):

$$Z_{in} = Z_0\sqrt{\mu/\varepsilon}\tanh\left[j\frac{2\pi f d\sqrt{\mu\varepsilon}}{c}\right], \tag{4}$$

where Z_0 represents the free space's intrinsic impedance, μ denotes the sample's complex relative permeability, ε represents the relative complex permittivity, f denotes the electromagnetic wave's frequency, d represents absorber thickness, and c is the vacuum velocity of light.

The frequency dependency of the RLs for the sample at varying temperatures in the X band was determined using Eqs. 3, 4 and plotted in Figure 5 Different colors represent the RL curve at corresponding temperatures. According to the theoretical formula, when the thickness is 5 mm, the RL of

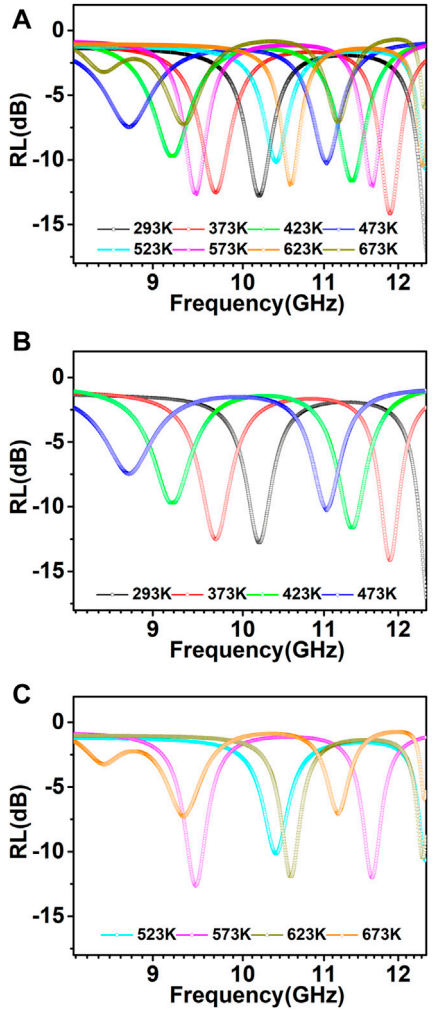

FIGURE 5
The temperature dependence microwave absorption performance of the sample, **(A)** when the temperature change from 293K to 673K; **(B)** when the temperature change from 293K to 473K; **(C)** when the temperature change from 523K to 673K.

the sample can be less than -10dB. Moreover, it is revealed that the minimum value of the sample's RL can be less than -10dB in the entire X band from ambient temperature to 623 K; when the temperature reached 673K, it began to deteriorate. As the temperature rose to 673K, there were two or three peaks seen in all samples' RL curves. Additionally, as the temperature rose to 623K, the frequency of RL peaks shifted to the low-frequency direction. When the temperature was raised to 673K, this sample demonstrated remarkable microwave absorption efficiency. During the whole test, it was held for 15 min at each temperature point. In the entire X band, the absorption performance has almost remained unaltered and is still effective. The outcome demonstrated that $SrFe_{12}O_{19}$ absorbing materials may retain stable RL performance at elevated temperatures. In addition, the temperature of $SrFe_{12}O_{19}$ absorbing material can be regulated to achieve the control of the absorbing frequency band within the 8–12 GHz frequency range.

Conclusion

In conclusion, $SrFe_{12}O_{19}$ hexaferrites have been successfully produced using the molten salt process, and the microstructure, magnetic characteristics, and microwave properties have been examined in depth. The XRD analysis revealed that the lattice parameters of $SrFe_{12}O_{19}$ exhibit a typical hexagonal surface morphology. In particular, we evaluated systematically the changes in electromagnetic characteristics and microwave absorption performance of $SrFe_{12}O_{19}$ in the X band at 293–673 K. Temperature increased both the real components of permittivity and permeability. The temperature had no discernible effect on either the permittivity or permeability of imaginary parts. As the temperature increased to 673K, two or three peaks could be detected in the RL curves of all samples. In addition, as the temperature reached 623K, the frequency of RL peaks shifted towards low-frequency. In the X band from ambient temperature to 623 K, the minimum value of the sample's RL can be less than -10dB. All of the results showed that an absorber loaded with $SrFe_{12}O_{19}$ particles can be used in a high-temperature environment and perform well in terms of absorption. In addition, the temperature of $SrFe_{12}O_{19}$ absorbing material can be regulated to achieve the control of the absorbing frequency band within the 8–12 GHz frequency range.

Data availability statement

The original contributions presented in the study are included in the article/supplementary material, further inquiries can be directed to the corresponding author.

Author contributions

All authors listed have made a substantial, direct, and intellectual contribution to the work and approved it for publication.

Funding

This work was supported by the National Natural Science Foundation of China (Grant Nos. 91963201, 12074158 and 51771086), Natural Science Foundation of GanSu Province for Distinguished Young Scholars (No. 20JR10RA649), Open Project of Key Laboratory for Magnetism and Magnetic Materials of the Ministry of Education, Lanzhou University, China (Grant No. LZUMMM2021002), and the Fundamental Research Funds for

the Central Universities of Lanzhou University, China (Grant No. lzujbky-2021-kb06).

Conflict of interest

The authors declare that the research was conducted in the absence of any commercial or financial relationships that could be construed as a potential conflict of interest.

Publisher's note

All claims expressed in this article are solely those of the authors and do not necessarily represent those of their affiliated organizations, or those of the publisher, the editors and the reviewers. Any product that may be evaluated in this article, or claim that may be made by its manufacturer, is not guaranteed or endorsed by the publisher.

References

Atwater, J., and Wheeler, R., Jr. (2004). Microwave permittivity and dielectric relaxation of a high surface area activated carbon. *Appl. Phys. A* 79, 79125–79129. doi:10.1007/s00339-003-2329-8

Buzinaro, M. M. P., Ferreira, N. S., Cunha, F., and Macedo, M. A. (2016). Hopkinson effect, structural and magnetic properties of M-type Sm3+-doped SrFe12O19 nanoparticles produced by a proteic sol–gel process. *Ceram. Int.* 42, 5865–5872. doi:10.1016/j.ceramint.2015.12.130

Cao, M. S., Song, W. L., Hou, Z. L., Wen, B., and Yuan, J. (2010). The effects of temperature and frequency on the dielectric properties, electromagnetic interference shielding and microwave-absorption of short carbon fiber/silica composites. *Carbon* 48, 788–796. doi:10.1016/j.carbon.2009.10.028

Correia, N. T., and Ramos, J. M. (2000). On the cooperativity of the β-relaxation: A discussion based on dielectric relaxation and thermally stimulated depolarisation currents data. *Phys. Chem. Chem. Phys.* 2, 5712–5715. doi:10.1039/B005867J

Fathi, M., Mehdipour, M., and Shokrollahi, H. J. (2020). Microwave absorption properties of nanostructure composite particles based on SrFe12O19. *J. Aust. Ceram. Soc.* 56, 251–256. doi:10.1007/s41779-019-00414-7

Ghasemi, A., Hossienpour, A., Morisako, A., Saatchi, A., and Salehi, M. (2006). Electromagnetic properties and microwave absorbing characteristics of doped barium hexaferrite. *J. Magn. Magn. Mat.* 302, 429–435. doi:10.1016/j.jmmm.2005.10.006

Ghasemi, A., and Mousavinia, M. (2014). Structural and magnetic evaluation of substituted NiZnFe2O4 particles synthesized by conventional sol–gel method. *Ceram. Int.* 40, 2825–2834. doi:10.1016/j.ceramint.2013.10.031

Guan, X. Y., Yang, Z. H., Zhou, M., Yang, L., Peymanfar, R., Aslibeiki, B., et al. (2022). 2D MXene nanomaterials: Synthesis, mechanism, and multifunctional applications in microwave absorption. *Small Struct.* 3, 2200102. doi:10.1002/sstr.202200102

Li, L. Z., Wei, J. Z., Xia, Y. H., Wu, R., Yun, C., Yang, Y. B., et al. (2014). High frequency electromagnetic properties of interstitial-atom-modified Ce2Fe17NX and its composites. *Appl. Phys. Lett.* 105, 022902. doi:10.1063/1.4889806

Li, Q. F., Yan, S. Q., Wang, X., Nie, Y., Feng, Z. K., Su, Z. J., et al. (2015). Dual-ion substitution induced high impedance of Co2Z hexaferrites for ultra-high frequency applications. *Acta Mat.* 98, 190–196. doi:10.1016/j.actamat.2015.07.038

Li, Y., Cao, M. S., Wang, D. W., and Yuan, J. (2015). High-efficiency and dynamic stable electromagnetic wave attenuation for La doped bismuth ferrite at elevated temperature and gigahertz frequency. *RSC Adv.* 5, 77184–77191. doi:10.1039/c5ra15458h

Li, Y., Fang, X. Y., and Cao, M. S. (2016). Thermal frequency shift and tunable microwave absorption in BiFeO3 family. *Sci. Rep.* 6, 24837. doi:10.1038/srep24837

Li, Y., Sun, N. N., Liu, J., Hao, X. H., Du, J. H., Yang, H. J., et al. (2018). Multifunctional BiFeO3 composites: Absorption attenuation dominated effective electromagnetic interference shielding and electromagnetic absorption induced by multiple dielectric and magnetic relaxations. *Compos. Sci. Technol.* 159, 240–250. doi:10.1016/j.compscitech.2018.02.014

Li, Y., Wang, G. C., Gong, A., Zhang, S., Liu, J., Sun, N. N., et al. (2022). High-performance ferroelectric electromagnetic attenuation materials with multiple polar units based on nanodomain engineering. *Small* 18, 2106302. doi:10.1002/smll.202106302

Li, Y., Yang, H. J., Hao, X. H., Sun, N. N., Du, J. H., and Cao, M. S. (2019). Enhanced electromagnetic interference shielding with low reflection induced by heterogeneous double-layer structure in BiFeO3/BaFe7(MnTi)2.5O19 composite. *J. Alloys Compd.* 772, 99–104. doi:10.1016/j.jallcom.2018.09.047

Lu, M. M., Wang, X. X., Cao, W. Q., Yuan, J., and Cao, M. S. (2016). Carbon nanotube-CdS core–shell nanowires with tunable and high-efficiency microwave absorption at elevated temperature. *Nanotechnology* 27, 065702. doi:10.1088/0957-4484/27/6/065702

Luo, H., Tan, Y. Q., Li, Y., Xiao, P., Deng, L. W., Zeng, S. F., et al. (2017). Modeling for high-temperature dielectric behavior of multilayer C/Si3N4 composites in X-band. *J. Eur. Ceram. Soc.* 37, 1961–1968. doi:10.1016/j.jeurceramsoc.2016.12.028

Mehdipour, M., and Shokrollahi, H. J. (2013). Comparison of microwave absorption properties of SrFe12O19, SrFe12O19/NiFe2O4, and NiFe2O4 particles. *J. Appl. Phys.* 114, 043906. doi:10.1063/1.4816089

Mu, Z. G., Wei, G. K., Zhang, H., Gao, L., Zhao, Y., Tang, S. L., et al. (2022). The dielectric behavior and efficient microwave absorption of doped nanoscale $LaMnO_3$ at elevated temperature. *Nano Res.* 15, 7731–7741. doi:10.1007/s12274-022-4500-6

Naito, Y., and Suetake, K. (1971). Application of ferrite to electromagnetic wave absorber and its characteristics. *IEEE Trans. Microw. Theory Tech.* 19, 65–72. doi:10.1109/TMTT.1971.1127446

Nayak, L., Khastgir, D., and Chaki, T. K. (2013). A mechanistic study on electromagnetic shielding effectiveness of polysulfone/carbon nanofibers nanocomposites. *J. Mat. Sci.* 48, 1492–1502. doi:10.1007/s10853-012-6904-2

Nie, Y., Harward, I., Balin, K., Beaubien, A., and Celinski, Z. (2010). Preparation and characterization of barium hexagonal ferrite thin films on a Pt template. *J. Appl. Phys.* 107, 073903. doi:10.1063/1.3343567

Shi, X. L., Cao, M. S., Fang, X. Y., Yuan, J., Kang, Y. Q., and Song, W. L. (2008). High-temperature dielectric properties and enhanced temperature-response attenuation of β-MnO2 nanorods. *Appl. Phys. Lett.* 93, 223112. doi:10.1063/1.3042210

Song, W. L., Cao, M. S., Hou, Z. L., Fang, X. Y., Shi, X. L., and Yuan, J. (2009). High dielectric loss and its monotonic dependence of conducting-dominated multiwalled carbon nanotubes/silica nanocomposite on temperature ranging from 373 to 873 K in XX-band. *Appl. Phys. Lett.* 94, 233110. doi:10.1063/1.3152764

Stumper, U., and Schrader, T. (2014). Calibration method for vector network analyzers using one or two known reflection standards. *IEEE Trans. Instrum. Meas.* 63, 1648–1655. doi:10.1109/TIM.2013.2292754

Tang, X. T., Wei, G. T., Zhu, T. X., Sheng, L. M., An, K., Yu, L. M., et al. (2016). Microwave absorption performance enhanced by high-crystalline graphene and BaFe12O19 nanocomposites. *J. Appl. Phys.* 119, 204301. doi:10.1063/1.4951002

Wang, J. F., Ponton, C. B., and Harris, I. R. (2001). A study of the magnetic properties of hydrothermally synthesised Sr hexaferrite with Sm substitution. *J. Magn. Magn. Mat.* 234, 233–240. doi:10.1016/S0304-8853(01)00366-3

Wessling, B. (1991). Electrical conductivity in heterogeneous polymer systems. V (1): Further experimental evidence for a phase transition at the critical volume concentration. *Polym. Eng. Sci.* 31, 1200–1206. doi:10.1002/pen.760311608

Ye, W. C., Fu, J. J., Wang, Q., Wang, C. M., and Xue, D. S. (2015). Electromagnetic wave absorption properties of NiCoP alloy nanoparticles decorated on reduced graphene oxide nanosheets. *J. Magn. Magn. Mat.* 395, 147–151. doi:10.1016/j.jmmm.2015.07.087

Yuan, X. Y., Cheng, L. F., Guo, S. W., and Zhang, L. T. (2017). High-temperature microwave absorbing properties of ordered mesoporous inter-filled SiC/SiO2 composites. *Ceram. Int.* 43, 282–288. doi:10.1016/j.ceramint.2016.09.151

Zhang, D. F., Hao, Z. F., Zeng, B., Qian, Y. N., Huang, Y. X., and Yang, Z. D. (2016). Theoretical calculation and experiment of microwave electromagnetic property of Ni(C) nanocapsules. *Chin. Phys. B* 25, 040201. doi:10.1088/1674-1056/25/4/040201

Zheng, D. L., Liu, T., Zhou, L., and Xu, Y. G. (2016). Electromagnetic absorbing property of the flaky carbonyl iron particles by chemical corrosion process. *J. Magn. Magn. Mat.* 419, 119–124. doi:10.1016/j.jmmm.2016.06.008

Zi, Z. F., Sun, Y. P., Zhu, X. B., Yang, Z. R., Dai, J. M., and Song, W. H. (2009). Synthesis of magnetoresistive La0.7Sr0.3MnO3 nanoparticles by an improved chemical coprecipitation method. *J. Magn. Magn. Mat.* 321, 2378–2381. doi:10.1016/j.jmmm.2009.02.130